Chapter 11

Physics of High-Density Radio Frequency Capacitively Coupled Plasma with Various Electrodes and Its Applications

Yasunori Ohtsu

Additional information is available at the end of the chapter

http://dx.doi.org/10.5772/intechopen.78387

Abstract

The radio frequency discharge plasma sources are widely utilized to prepare functional thin films and to etch insulated layers in semiconductor devices in microelectronic industry. Especially, a capacitively coupled plasma (CCP) is the most popular discharge because the equipment is very simple and almost maintenance free. However, there is a problem such as low-density plasma under low-gas pressure less than 10 Pa, that is, low processing rate. In this chapter, the production principle of conventional CCP and the special CCP with various electrodes and magnets is reviewed. The applications prepared by the special CCP system are also presented. Finally, the future plan including problems is described.

Keywords: RF plasma, capacitively coupled plasma, plasma processing, hollow cathode discharge, ring-shaped hollow plasma, magnetized plasma

1. Introduction

A large-scale integrated circuit (LSI), various sensors, and other semiconductor devices are essential for various electrical and electronic devices and automobile [1, 2]. In general, these devices are fabricated by plasma-processing techniques such as dry etching and plasma deposition using low-pressure plasma. The plasma processing is the most usually utilized chemical and physical processes in microelectronics fabrication for functional thin film preparation and dry etching of silicon-based films.

In the dry-etching processing, the silicon wafer patterned by the photoresist mask for LSI is exposed in plasma containing halogen molecules (e.g., CF_4, CHF_3, SF_6) [3–7]. In the case of these gases, the fluorine atoms dissociated by an electron impact collision with the molecules react with the silicon surface to generate a volatile etch product like SiF_4 so that the silicon wafer is etched with assistance of energetic ions produced in the plasma. For example, a high-density plasma sources have been developed to challenge patterning features less than 0.25 μm with high aspect ratios [8].

The plasma deposition has a sputtering deposition and a plasma-enhanced chemical vapor deposition (PECVD) method. The sputtering deposition is to impinge ions to the material target biased by a negative potential so as to sputter atoms from the target. The functional thin films such as transparent conductive oxide used in tableted computer and smartphone are deposited by sputtering method [9]. The sputtering depositions are prepared by DC magnetron and radio frequency (RF) magnetron plasma sources [10]. Various typed sputtering sources have been developed for the synthesis of high-quality thin films [10]. Especially, RF magnetron plasma source has an advantage that the insulated films can be deposited on the various substrates compared with DC magnetron plasma source. The PECVD is to dissociate molecule by electron impact so as to deposit radicals [8].

In these plasma-processing techniques, capacitively coupled plasma (CCP) with parallel plates was widely utilized. The physics of CCP has been studied by many researchers [11–16]. The sustaining mechanism of CCP is the electron heating process that the oscillating radio frequency sheath near the powered electrode plays an important role in electron acceleration as well as the collisional heating in the presence of electric fields and the emission process of secondary electrons from the electrode [11–16]. However, the electron heating process cannot produce high-density plasma.

The requirement of these semiconductor devices with high-speed operation and high performance is increasing annually. In order to perform the demand, high-speed plasma processing, that is, a high-density plasma production, is important. However, CCP does not attain high-density plasma. Thus, the high-density CCP is required. In this chapter, the production principle of conventional CCP and the special CCP with various electrodes and magnets is reviewed.

2. Production principle of conventional capacitively coupled plasma

In order to perform the high-speed processing of the LSI semiconductor, high-density plasma is needed for CCP. The power balance of CCP in the form of a global model [17] is expressed as the following equation:

$$P_{ab} = en_e u_B S(\varepsilon_e + \varepsilon_i + \varepsilon_c). \quad (1)$$

Here, P_{ab}, e, u_B, and S are the total absorbed power, the electronic charge, the Bohm velocity, and the surface area, respectively. ε_e and ε_i are the averaged energy loss per electron and ion

lost to the electrodes. ε_c denotes the collisional energy loss per electron-ion pair created. The plasma density, n_e, can be determined from Eq. (1)

$$n_e = \frac{P_{ab}}{en_e S(\varepsilon_e + \varepsilon_i + \varepsilon_c)}. \quad (2)$$

When only thermal electrons are lost to the boundary surfaces [18], ε_e will be negligible. In general, the electron temperature decreases with increasing gas pressure [17]. Then, ε_c increases, while ε_i regularly decreases with increasing gas pressure, because the sheath is more collisional. For a fixed absorbed power, the increase in the plasma density is resulted with increasing gas pressure. Even for a relatively high-gas pressure of 50 Pa used in RF PECVD, however, the plasma density at a conventional driving frequency of 13.56 MHz is less than 10^{10} cm^{-3}.

In order to increase the plasma density at the typical frequency of 13.56 MHz, ingenious device is required. In the next section, the various ingenuities will be introduced.

3. Effect of high secondary electron emission oxide on high-density capacitively coupled plasma production

In general, plasma is generated by electrons with an energy higher than an ionization potential of target neutral gas [19]. According to the ionization cross section [20] for noble gases of He, Ne, Ar, and Xe, their ionization energy ranges from 10 to 30 eV, while the energy is a few 100 electron volts when the ionization cross section becomes maximum. These electrons are effectively possible to ionize neutral gases through inelastic collisions. Then, it is expected to produce high-density plasma. In CCP discharge, it is also easy to generate a high voltage of a few hundred volts between the powered and grounded electrodes, that is, CCP can generate secondary electron emission (SEE) from the powered electrode. It was reported that magnesium oxide (MgO) electrodes have a high SEE coefficient which are a few 10 times higher than that of conventional metal electrodes such as aluminum [21].

In this section, the effect of SEE as the acceleration mechanism of electrons is proposed to solve the serious problem of CCP density. The RF breakdown voltage and plasma density are studied experimentally. As show in **Figure 1(a)**, an RF power of 13.56 MHz was supplied to generate CCP between two electrodes of 20-mm diameter with a gap d_{gap} of 10 mm, which were mounted into the center of a cylindrical vessel of 160-mm diameter and 200-mm length. The back of the RF electrode is covered by a grounded metal enclosure to avoid additional discharge between the RF electrode and the grounded vessel. An MgO disk of 20-mm diameter and 2-mm thickness was connected to the Al metal electrode, as shown in **Figure 1(b)**. As a working gas, Ne or Ar gas was introduced in the vessel at 133 Pa.

Figure 2 shows RF breakdown voltage V_{Brf} characteristics. V_{Brf} is expressed as a peak-to-peak value measured by a high voltage probe and a digital oscilloscope. V_{Brf} characteristics exhibit a roughly U-shaped distribution like Paschen's curve of Townsend discharge [22] for both Ne

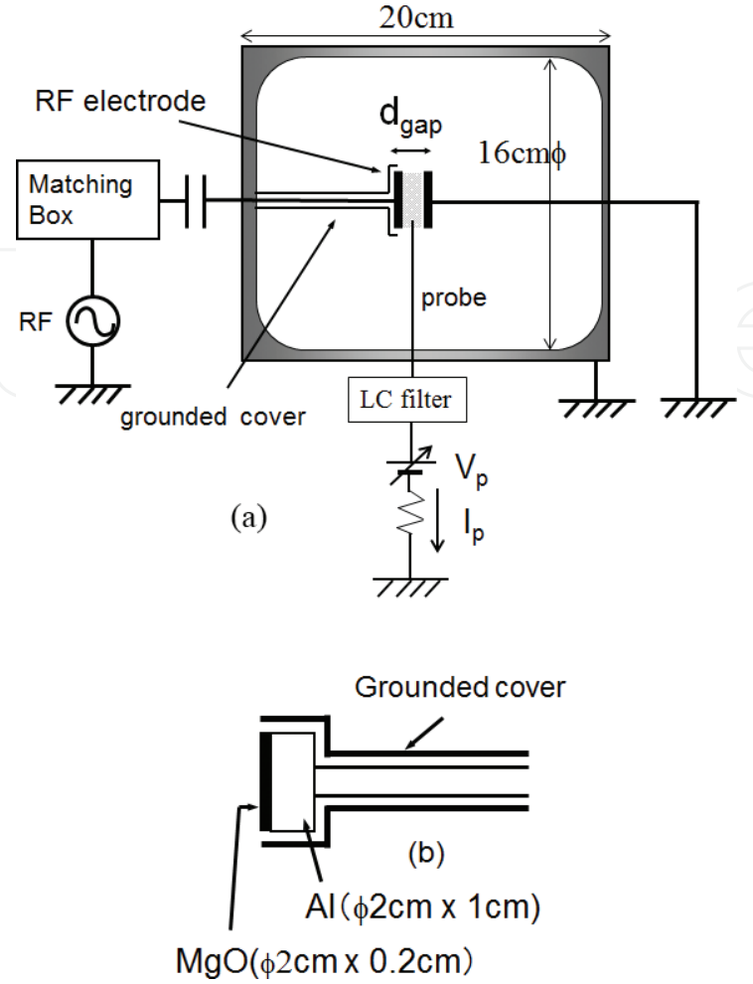

Figure 1. (a) Experimental apparatus and (b) electrode construction.

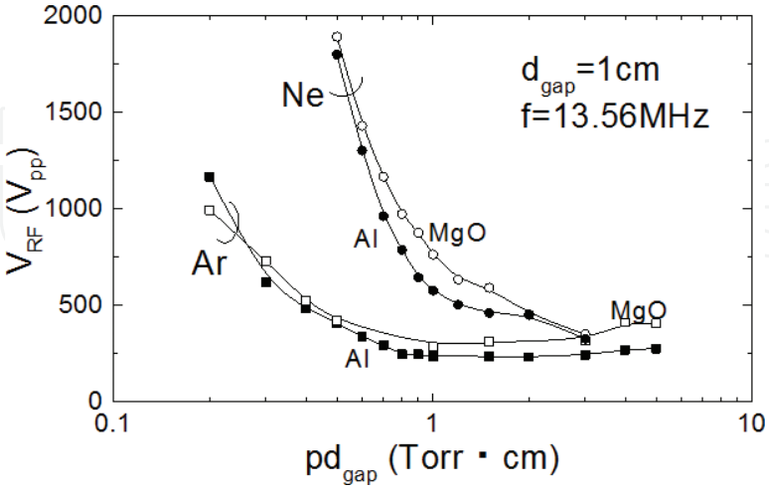

Figure 2. Breakdown voltage V_{RF} as a function of pd_{gap}. Here, p and d_{gap} denote gas pressure and gap distance, respectively.

and Ar gases. It is found that V_{Brf} for MgO electrode is higher than that for Al electrode for both Ne and Ar gases, whereas it is reported [21] that the coefficient of SEE for MgO is higher than that for Al. This is ascribed by the effect of voltage drop across MgO. It is also observed

http://dx.doi.org/10.5772/intechopen.78387

that V_{Brf} for Ar gas is lower than that for Ne gas because the ionization potential of Ar gas is lower than that of Ne gas [20].

Figure 3 shows plasma density j_{is} as a function of RF voltage V_{RF} applied between the RF electrode and the grounded vessel. The plasma density was estimated from an ion saturation current density j_{is} [23] measured by a tiny Langmuir probe to avoid the disturbance of the plasma by the probe. This is because the electron temperature was almost constant as a function of the RF voltage. The solid line shown in **Figure 3** corresponds to j_{is} when it is proportional to V_{RF}. The value of $j_{is} = 8 \times 10^{-3}$ A/cm^2 is almost an electron density of approximately 10^{10} cm^{-3}. As mentioned in **Figure 3**, the breakdown voltage V_{Brf} for Ne gas at both MgO and Al electrodes ranged from 500 to 1750 V_{pp}. For Al electrode, it is found that plasma density increases roughly proportionally to V_{RF}. The plasma density is only of the order of 10^9 cm^{-3} at even $V_{RF} = 1$ kV$_{pp}$.

According to the scaling law under the assumption that the stochastic heating without the SEE effect in the main discharge mechanism in CCP [17], the plasma density can be expressed as

$$n_e \propto \omega^2 V_{RF}/\varepsilon, \tag{3}$$

where ω, V_{RF}, and ε are the angular driving frequency, the RF voltage, and the energy needed to generate electrons and ions, respectively. Eq. (3) expresses that n_e is proportional to V_{RF} under the experiment that ω and ε are fixed. In the case of Al electrode, the experimental data almost correspond to the line of $n_e \propto \omega$. That is, the plasma production without SEE effect is predominant by stochastic heating where electrons accelerated by the oscillating RF sheath ionize neutral particles.

For MgO electrode, the plasma density is one order of magnitude higher than that for Al electrode. It is found that plasma density increases obviously with increasing V_{RF} for $V_{RF} > 400$ V_{pp}, and then attained over 10^{10} cm^{-3} for $V_{RF} > 800$ V_{pp} and then saturates. The SEE energy emitted from the MgO electrode corresponds to approximately 200 eV at $V_{RF} = 400$ V_{pp}. For electron-Ne

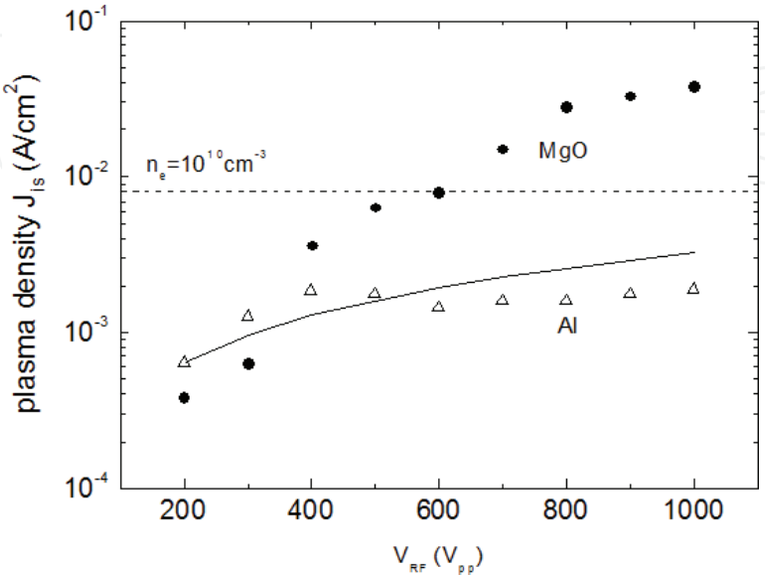

Figure 3. Plasma density j_{is} as a function of V_{RF} for Al and MgO electrodes. The solid line is the line of $n_e \propto \omega$.

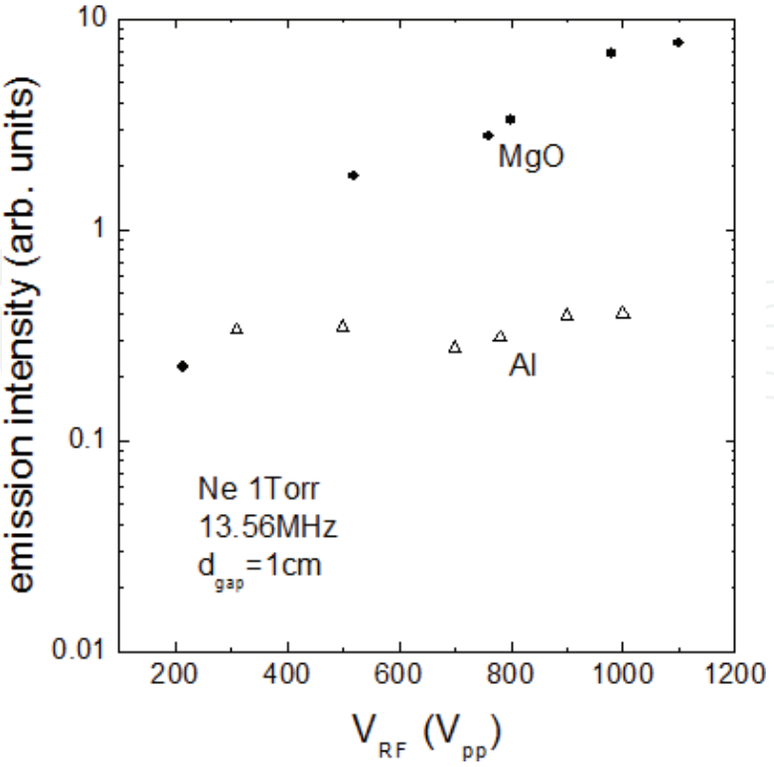

Figure 4. Optical emission intensity of He I line (588.1 nm) as a function of V_{RF}.

gas inelastic collision, this SEE energy of E_{SEE} = 200 eV has the maximum ionization cross section [20]. Thus, for V_{RF} > 400 V_{pp}, the ionization of Ne gas is effectively enhanced by the high SEE coefficient of MgO [21], which leads to the marked increase of plasma density. In fact, the RF power input to the plasma for MgO was higher than that for Al at a fixed applied voltage. Unfortunately, the power efficiency of the reactor could not be estimated because it was not easy to directly monitor current and phase difference between voltage and current.

The reason why the plasma density for MgO becomes constant for V_{RF} > 800 V_{pp} is considered as follows. The ionization cross section starts to decrease with increasing E_{SEE} for E_{SEE} > 400 eV [20]. Thus, the plasma density decreases with increasing V_{RF} for V_{RF} > 800 V_{pp}.

Figure 4 shows optical emission intensity of the Ne I line (588.1 nm) as a function of V_{RF}. Here, the optical emission intensity was measured with a spectrometer and a digital oscilloscope. The intensity increases markedly with increasing V_{RF}, in the same manner as plasma density. Therefore, the high-density plasma production is realized by using MgO with a high SEE coefficient in CCP. The effect of high secondary electron emission is one candidate to produce high-density plasma.

4. Effect of structured electrodes on high-density capacitively coupled plasma production

In this section, it is described that structured electrodes can produce the high-density capacitively coupled plasma. One of the structured electrodes is a hollow cathode. The hollow cathode discharge [24] is applied into a production mechanism of CCP to attain high-density plasma.

4.1. Multi-hollow electrode

The effects of a multi-hollow cathode discharge and a high SEE are applied to capacitively coupled plasma to produce high-density plasma [25, 26]. **Figure 5(a)** and **(b)** shows the experimental apparatus and construction of the multi-hollow electrode, respectively. As shown in **Figure 5(b)**, one plate has 35 holes with 5-mm diameter and 15-mm length, and these holes lay on a concentric circle. In order to emit secondary electron emission from the electrode facing the multi-hollow electrode, the other electrode is biased by the voltage of low frequency of 1 MHz. The plate is called as the substrate electrode.

Figure 6 shows plasma density and electron-neutral mean free path as a function of Ar gas pressure. Here, plasma density was estimated by ion saturation current density of a negatively biased probe because plasma density is proportional to ion saturation current [27]. The electron-neutral mean free path λ_{en} was also calculated by the following equation:

$$\lambda_{en} = (\sigma n)^{-1}, \tag{4}$$

where σ and n are electro-neutral cross section and Ar gas density, respectively. In **Figure 6**, as a reference value, an absolute value of the plasma density for Ar gas pressure 37.5 mTorr was estimated from electron saturation current density of probe and is approximately 8×10^{10} cm^{-3}. The plasma density drastically increases with an increasing gas pressure from 7.5 to 22.6 mTorr Pa and then varies by order, although the electron-neutral mean free path is inversely proportional to the gas pressure and reaches the hole size of 5 mm at the gas pressure of 113 mTorr. It is confirmed that the hollow cathode effect is achieved at the pressure range of 22.6–112.5 mTorr where the mean free path is comparable to the hole size of 5 mm.

The effect of SEE to attain high-density plasma production was examined by biasing the substrate electrode. **Figure 7** shows plasma density as a function of substrate biasing voltage V_b for axial position $z = 5$ mm and radial position $r = 0$ where the origins of z and r are the surface and the center of the powered electrode, respectively. The dashed line denotes the absolute value of plasma density for $V_b = 0$, which was estimated to be approximately 10^{10} cm^{-3} from probe characteristics. It is seen that plasma density increases with the substrate-biased voltage V_b and approached approximately 10^{11} cm^{-3} at $V_b = -800$ V. This suggests that the increase in V_b performs to ionize neutral atoms by inelastic collisions of secondary high-energy electrons. The film preparation is tried by using methane gas. **Figure 8** shows the deposition rate as a function of substrate biased voltage V_b. It is found that the deposition rate exponentially increases with increasing V_b in the range of $100 < V_b < 500$ V and then saturates. This is because the hybrid discharge combines the hollow cathode discharge and the secondary electron emission. Therefore, the drastic increase in the deposition rate is ascribed by realizing this hybrid discharge. For $V_b > 300$ V, the deposition rate exceeds the previous reported maximum value which is approximately 30 nm/min [28]. The deposition rate of 200 nm/min is attained at $V_b > 500$ V.

4.2. Ring-shaped hollow electrode

In the previous subsection, the effect of multi-hollow electrode on high-density capacitively coupled plasma was described [29]. In this subsection, the ring-shaped hollow electrode was tried to produce high-density capacitively coupled plasma. The high-density plasma in the

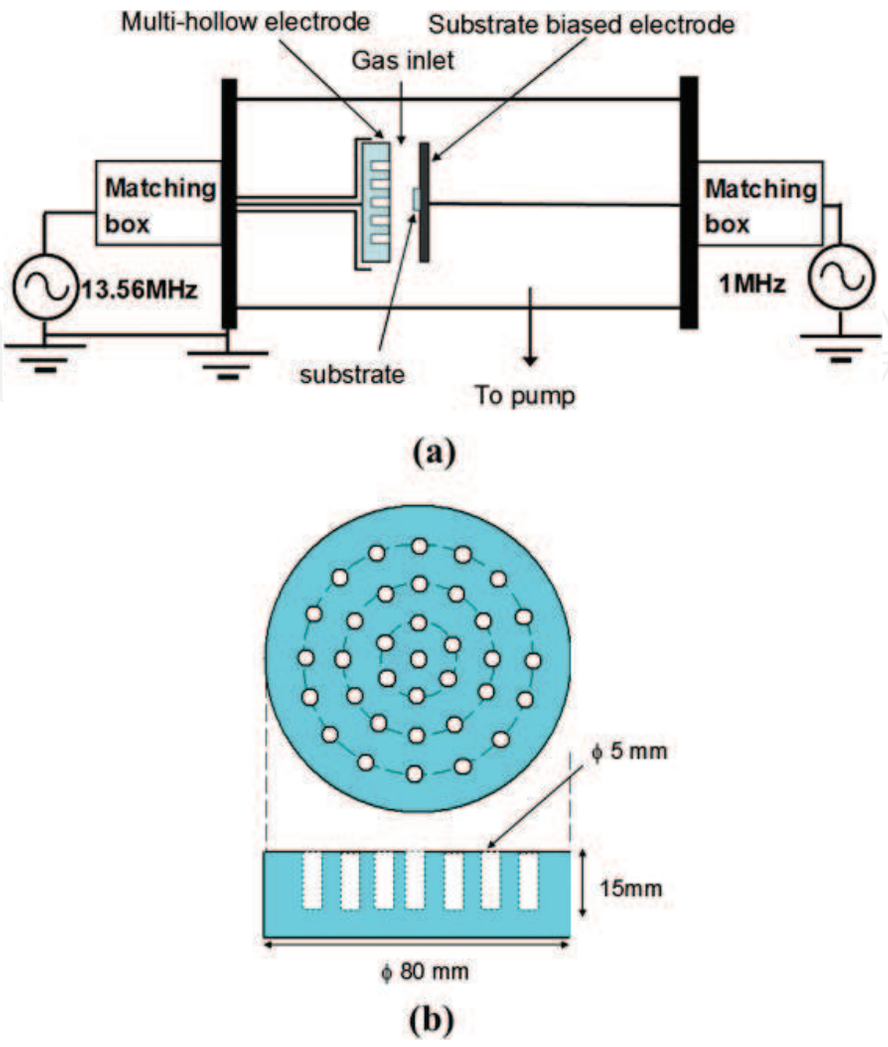

Figure 5. (a) Experimental apparatus and (b) construction of multi-hollow electrode.

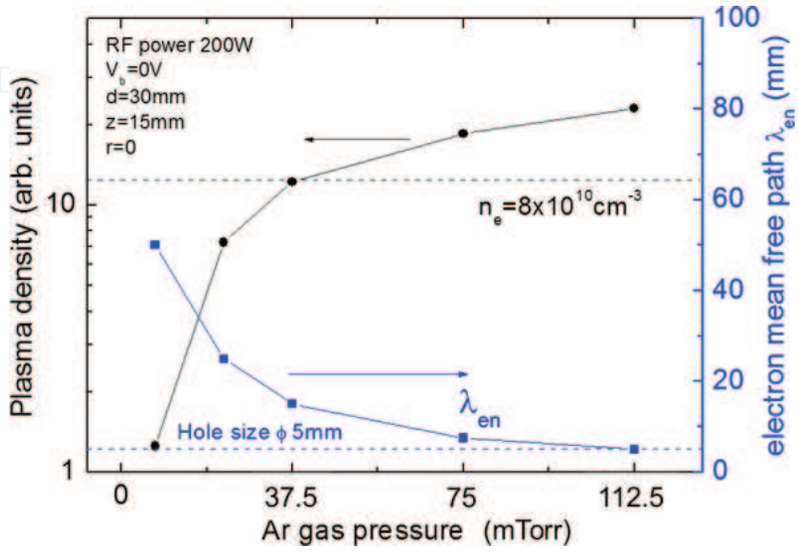

Figure 6. Plasma density and electron-neutral mean free path as a function of Ar gas pressure.

http://dx.doi.org/10.5772/intechopen.78387

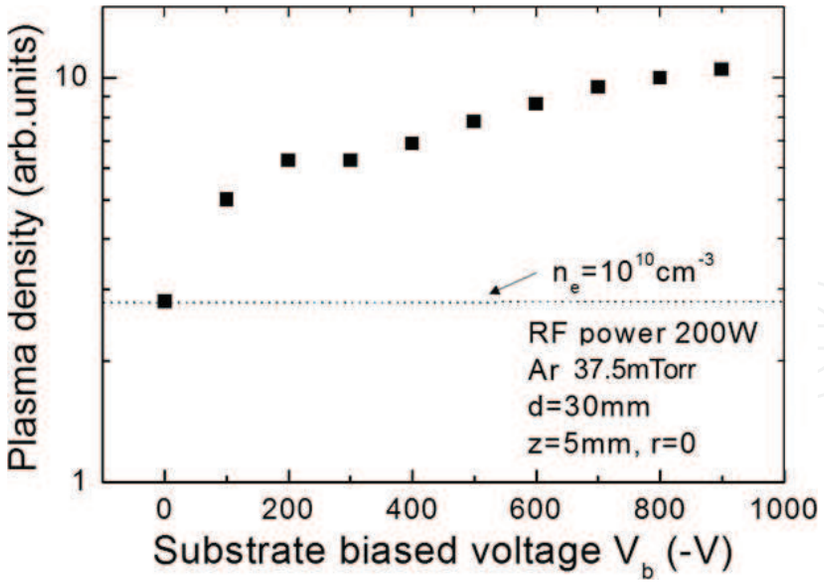

Figure 7. Plasma density as a function of RF-biased voltage.

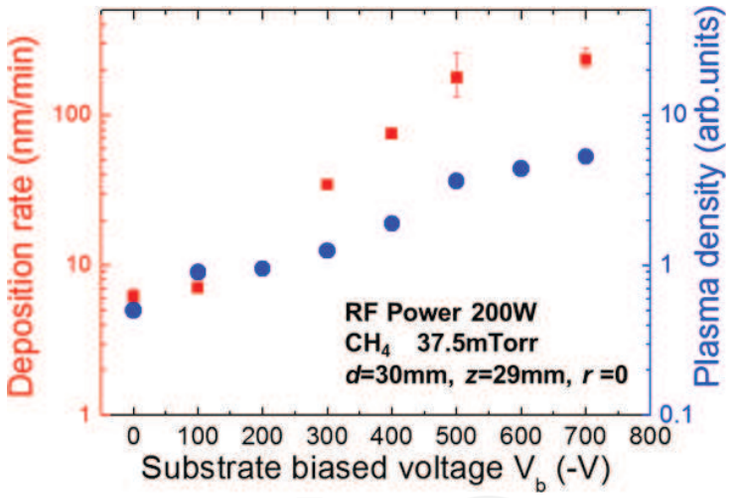

Figure 8. Deposition rate of thin films and plasma density as a function of RF-biased voltage.

trench diffuses toward the downstream region, and then the radial profile of plasma density becomes uniform at a certain axial position. The influence of trench width and gas pressure on plasma density and its profile is examined, comparing the case of a conventional flat electrode.

It is very important to accelerate electrons in the trench by moving RF cathode sheath for producing the high-density plasma with a hollow cathode effect. To satisfy the hollow cathode effect, it is required that the hollow trench width W be twice as long as the sheath thickness d_s as shown in **Figure 9(a)**. The depth of the hollow trench must be larger than the sheath thickness. In order to determine the trench width W, the sheath thickness d_s can be estimated by the following equation:

$$d_s = \frac{\sqrt{2}}{3}\lambda_D\left(\frac{2eV_{sh}}{T_e}\right)^{\frac{3}{4}}, \tag{5}$$

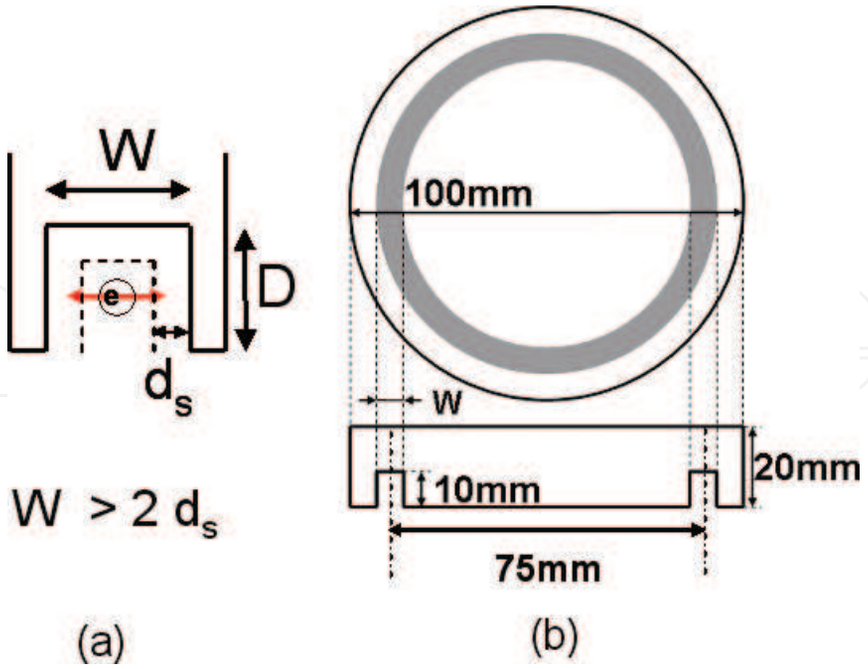

Figure 9. (a) Cross section near the ring-shaped trench and (b) structure of the RF hollow powered electrode.

where λ_D, $T_{e,}$ and V_{sh} denote the Debye length, the electron temperature, and the time-averaged sheath voltage of the RF electrode which was used as the typical self-biased voltage, respectively. Eq. (1) is derived from the Child-Langmuir Law [1, 11]. The sheath thickness d_s can be estimated to be approximately 2 mm by Eq. (4) using T_e = 4 eV, n_e = 10^{10} cm^{-3} and V_{sh} = 200 V. In this experiment, D is set at 5 and 10 mm. **Figure 9(b)** shows the cross section of the ring-shaped hollow electrode with 100-mm diameter and 20-mm thickness.

Figure 10(a) and **(b)** show typical images of plasma emission near the RF electrode for the ring-shaped hollow electrode and the flat electrode, respectively. As shown in **Figure 10(a)**, a high intensity of plasma emission is observed near the ring-shaped hollow trench for the ring-shaped hollow electrode. The hollow cathode effect is attained in the trench. On the other hand, the conventional flat electrode shows a uniform glow plasma on the whole electrode.

Figure 11 shows plasma density n_e as a function of Ar gas pressure p for the hollow and the flat electrodes. The position is fixed at z = 8 mm and r = 38 mm. For the hollow electrode, the plasma density raises rapidly with raising Ar gas pressure p and has a peak at p = 180 mTorr and then remains almost constant. At p = 350 mTorr, the plasma density decreases discontinuously, and then at p > 350 mTorr, the plasma density is independent of the gas pressure. The electron-neutral mean free path λ_{en} decreases with increasing gas pressure. λ_{en} at p = 350 mTorr is approximately 1 mm which is of the order of the magnitude of the hollow trench size. The maximum plasma density is approximately 2 × 10^{11} cm^{-3}. It is seen that the high-density plasma with the order of magnitude of 10^{11} cm^{-3} is achieved in a wide range of gas pressure from 100 to 300 mTorr. In the flat electrode, the plasma density shows a similar tendency with the hollow electrode. The maximum value of the plasma density is one order of magnitude lower than that of the hollow electrode.

http://dx.doi.org/10.5772/intechopen.78387

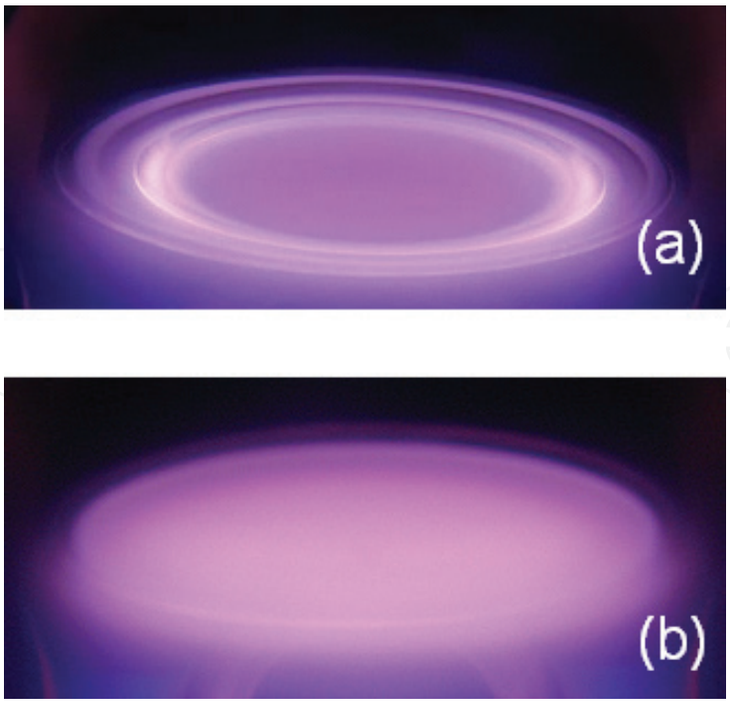

Figure 10. Typical images of plasma structure for (a) the hollow and (b) the flat electrodes.

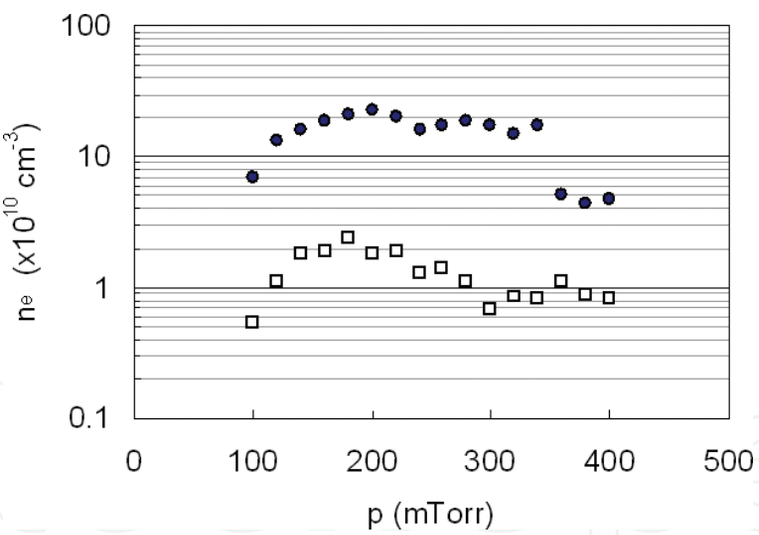

Figure 11. Plasma densities as a function of Ar gas pressure for the hollow (solid circles) and the flat electrodes (squares). Here, the ring-shaped trench width is $W = 5$ mm.

Figure 12 shows plasma density as a function of Ar gas pressure for $W = 5$ and 10 mm. Here, the measured position is at $z = 12$ mm and $r = 38$ mm. It is seen that the critical pressure when the plasma density attained 10^{11} cm^{-3} decreases with increasing the trench width. In fact, the critical values are 140 and 100 mTorr at $W = 5$ and 10 mm, respectively. The sheath thickness d_s was calculated to be approximately 1.7 mm at $n_e = 10^{11}$ cm^{-3} at the critical gas pressures. The condition of $W > 2d_s$ is satisfied at the critical gas pressure.

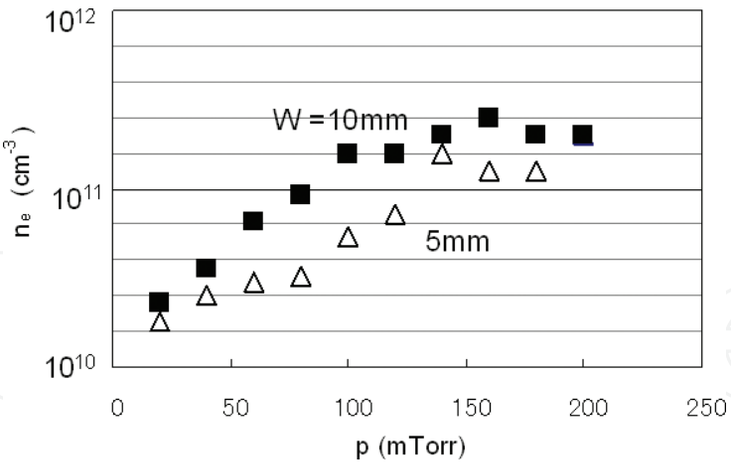

Figure 12. Plasma density as a function of Ar gas pressure at the hollow electrode for W = 5 and 10 mm under lower pressure conditions.

4.3. Magnetized ring-shaped hollow cathode discharge

In a low pressure of 1 Pa, it is difficult to produce plasma using only hollow cathode discharge [30]. In this subsection, in order to attain high-density plasma in the low-gas pressure, the combination of hollow cathode discharge and magnetic confinement with magnets is proposed. The addition of a magnetic field is one candidate for performing discharge in the low-gas pressure. It is easy to magnetize electrons under the low-gas pressure.

Figure 13 shows the construction of a ring-shaped hollow cathode for (a) the NS-NS arrangement, (b) the NS-SN arrangement, and (c) the NS arrangement of permanent magnets. The neodymium magnets were used. Three arrangements of permanent magnets were investigated. The NS-Ns arrangement is that two NS magnets with 7 × 10 mm^2 in cross section and 10 mm in length are positioned at both walls of a hollow trench and six couples of the NS-NS magnets are used as shown in **Figure 13(a)**. In the NS-SN arrangement, NS and SM magnets are mounted as shown in **Figure 13(b)**. As shown in **Figure 13(c)**, six NS magnets with 10 × 15 mm^2 in cross section and 6 mm in length are set at the bottom of a hollow trench for the NS arrangement. The outside of magnets is covered by iron yokes with 1 mm in thickness as shown in **Figure 13**.

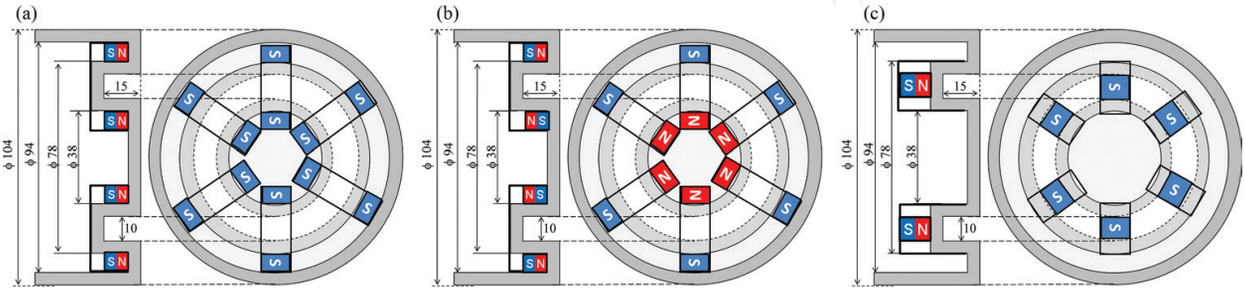

Figure 13. Constructions of a ring-shaped hollow cathode for (a) the NS-NS arrangement, (b) the NS-SN arrangement, and (c) the NS arrangement of permanent magnets. The neodymium magnets were used.

http://dx.doi.org/10.5772/intechopen.78387

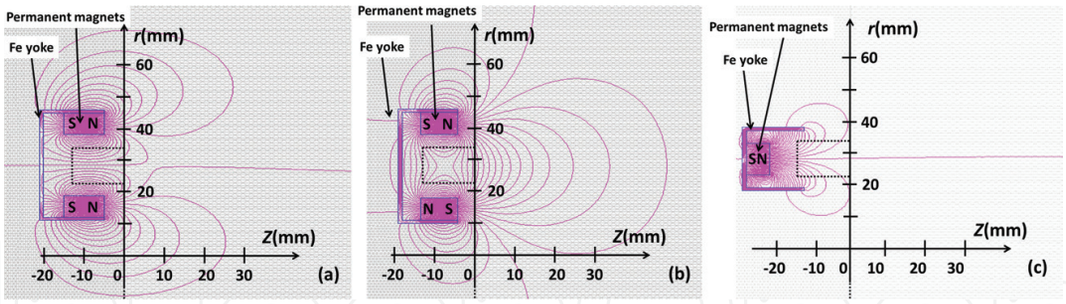

Figure 14. Two-dimensional distributions of magnetic field lines near the hollow cathode for (a) the NS-NS arrangement, (b) the NS-SN arrangement, and (c) the NS arrangement of the permanent magnets.

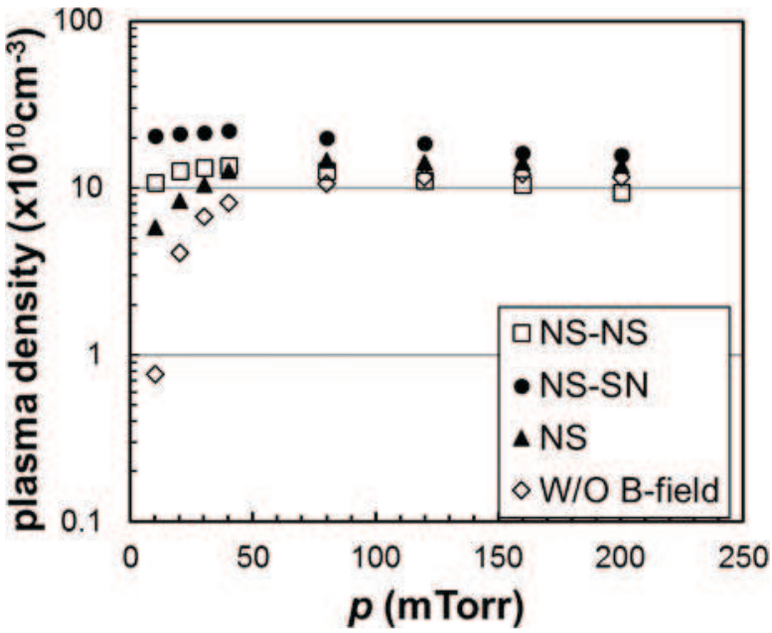

Figure 15. Plasma density as a function of Ar gas pressure at $r = 29$ mm and $z = 23$ mm at various magnet arrangements. Here, the data without magnetic field are also included for the comparison.

Figure 14 shows two-dimensional distributions of magnetic field lines at (a) NS-NS, (b) NS-SN, and (c) NS arrangements of permanent magnets, respectively. Here, the area enclosed by dashed lines is the hollow trench. As shown in **Figure 14(b)**, for the NS-SN arrangement, it is clear that the profile of the magnetic field lines is quite different from the other arrangement. The magnetic field lines show a cusp profile in the trench. The NS-SN arrangement is the best profile for magnetic confinement of electrons.

Figure 15 shows plasma density as a function of gas pressure at $r = 29$ mm and $z = 23$ mm at various arrangements. For the case without magnet, it is found that plasma density decreases from approximately 10^{11} cm^{-3} to 8×10^{9} cm^{-3} with a decreasing gas pressure less than 80 mTorr and saturates for a gas pressure region of 80–200 mTorr. It is difficult to sustain high-density plasma without magnet at a low-gas pressure. It is noticeable that the addition of magnets with hollow cathode discharge is effective for producing high-density plasma under the low-gas pressure. For the case of NS-SN arrangement, high-density plasma over 10^{11} cm^{-3} is achieved at all gas pressures.

In these chapters, in order to improve the plasma density in CCP, various typed CCP discharges have been presented. In Section 3, it is indicated that RF electrode with a high secondary electron emission oxide of MgO is effective to produce high-density capacitively coupled plasma. The plasma density for MgO electrode increases drastically with increasing RF voltage compared with the metal electrode of Al. In Section 4, it is described that the structured electrode plays an important role to improve the plasma density. This mechanism is ascribed by the hollow cathode effect.

5. Conclusions

The radio frequency capacitively coupled plasma source is widely utilized in the semiconductor fabrications. However, the source has a serious problem, although it has some merits such as simple structure and maintenance free. In this chapter, some solutions are introduced by adding simple methods. The first method is the high secondary electron emission electrode. The second method is multi-hollow and ring-shaped electrodes. The third method is magnetized ring-shaped electrode. All methods attained high-density plasma production. Especially, the ring-shaped electrode with magnets performed high-density plasma with 10^{11} cm^{-3} under a low-gas pressure. These methods will be useful to advance capacitively coupled plasma for microelectronic technology.

Author details

Yasunori Ohtsu

Address all correspondence to: ohtsuy@cc.saga-u.ac.jp

Faculty of Science and Engineering, Saga University, Saga, Japan

References

[1] Sugawara M, Stanfield BL, Handa S, Fujita H, Watanabe S, Tsukamoto T. Plasma Etching. Oxford University Press; 1998

[2] Roth JR. Industrial Plasma Engineering. Vol.2. Institute of Physics; 2001

[3] Heinecke RAH. Control of relative etch rates of SiO_2 and Si in plasma etching. Solid-State Electronics. 1975;**18**:1146

[4] Ephrath LM. Selective etching of silicon dioxide using reactive ion etching with CF_4-H_2. Journal of the Electrochemical Society. 1979;**126**:1419

[5] Coburn JW. In situ Auger electron spectroscopy of Si and SiO_2 surfaces plasma etched in CF_4-H_2 glow discharges. Journal of Applied Physics. 1979;**50**:5210

[6] Maruyama K, Sakai A, Goto T. Measurement of the CF_3 radical using infrared diode laser absorption spectroscopy. Journal of Physics D. 1993;**26**:199

[7] Maruyama K, Ohkouchi K, Ohtsu Y, Goto T. CF_3, CF_2 and CF Radical Measurements in RF CHF_3 Etching Plasma Using Infrared Diode Laser Absorption Spectroscopy. Japanese Journal of Applied Physics. 1994;**33**:4298

[8] Chen FF, Chang JP. Lecture Notes on Principles of Plasma Processing. Springer US; 2003

[9] Minami T, Nanto H, Tanaka S. Highly conductive and transparent zinc oxide films prepared by rf magnetron sputtering under an applied external magnetic field. Applied Physics Letters. 1982;**41**:958

[10] Musil J. Low-pressure magnetron sputtering. Vacuum. 1998;**50**:363

[11] Godyak VA, Piejak RB. Abnormally low electron energy and heating-mode transition in a low-pressure argon rf discharge at 13.56 MHz. Physical Review Letters. 1990;**65**:996

[12] Graves DB. Fluid model simulations of a 13.56-MHz rf discharge: Time and space dependence of rates of electron impact excitation. Journal of Applied Physics. 1987;**62**:88

[13] Goedde CG, Lichtenburg AJ, Lieberman MA. Self-consistent stochastic electron heating in radio frequency discharges. Journal of Applied Physics. 1988;**64**:4375

[14] Vender D, Boswell RW. Numerical modeling of low-pressure RF plasmas. IEEE Transactions on Plasma Sciences. 1990;**PS-18**:725

[15] Okuno Y, Ohtsu Y, Komatsu C, Fujita H. Measurement of electron energy distribution function in an asymmetric radio frequency discharge plasma. Journal of Applied Physics. 1993;**73**:1612

[16] Ohtsu Y, Okuno Y, Fujita H. Observation of radio-frequency discharges at various frequencies. Journal of Applied Physics. 1993;**73**:2155

[17] Lieberman MA, Lichitenberg AJ. Principle of Plasma Discharge and Materials Processing. 2nd ed. New Jersey: Wiley; 2005

[18] Liu YX, Gao F, Liu J, Wang YN. Experimental observation of standing wave effect in low-pressure very-high-frequency capacitive discharges. Journal of Applied Physics. 2014;**116**:043303

[19] Ohtsu Y, Fujita H. Production of high-density capacitively coupled radio-frequency discharge plasma by high-secondary-electron-emission oxide. Applied Physics Letters. 2004;**85**:4875. DOI: 10.1063/1.1827353

[20] Brown SC. Basic Data of Plasma Physics. 2nd ed. Revised. Cambridge: MIT; 1966

[21] Choi EH, Lim JY, Kim YG, Ko JJ, Kim DI, Lee CW, Cho GS. Secondary electron emission coefficient of a MgO single crystal. Journal of Applied Physics. 1999;**86**:6525

[22] Raizer YP, Shneider MN, Yatsenko NA. Radio-Frequency Capacitive Discharges. New York: CRC Press; 1995

[23] Chen FF. Plasma Diagnostic Techniques. New York: Academic; 1965

[24] Roth JR. Industrial Plasma Engineering. Principles. Vol. 1. Bristol: IoP; 1995

[25] Ohtsu Y, Fujita H. Production of high-density capacitive plasma by the effects of multihollow cathode discharge and high-secondary-electron emission. Applied Physics Letters. 2008;**92**:171501

[26] Ohtsu Y, Nakamura C, Misawa T, Fujita H, Akiyama M, Yukimura K. Production of high-density capacitively coupled plasma with RF multi-hollow cathode and/or high secondary electron emission for DLC film preparation. Plasma Processes and Polymers. 2009;**6**:S458-S461

[27] Hershkowitz N. How Langmuir Work. Plasma Diagnostics. Vol. 1. San Diego: Academic; 1989

[28] Robertson J. Diamond-like amorphous carbon. Materials Science and Engineering. 2002;**R37**:129

[29] Ohtsu Y, Urasaki H. Development of a high-density radio frequency plasma source with a ring-shaped trench hollow electrode for dry etching. Plasma Sources Science and Technology. 2010;**19**:045012 (6 pp)

[30] Ohtsu Y, Eguchi J, Yahata Y. Radio-frequency magnetized ring-shaped hollow cathode discharge plasma for low-pressure plasma processing. Vacuum. 2014;**101**:46-52